Decreased astroglial cell adhesion and proliferation on zinc oxide nanoparticle polyurethane composites

Justin T Seil
Thomas J Webster

Laboratory for Nanomedicine Research, Division of Engineering, Brown University, Providence, RI, USA

Abstract: Nanomaterials offer a number of properties that are of interest to the field of neural tissue engineering. Specifically, materials that exhibit nanoscale surface dimensions have been shown to promote neuron function while simultaneously minimizing the activity of cells such as astrocytes that inhibit central nervous system regeneration. Studies demonstrating enhanced neural tissue regeneration in electrical fields through the use of conductive materials have led to interest in piezoelectric materials (or those materials which generate a transient electrical potential when mechanically deformed) such as zinc oxide (ZnO). It has been speculated that ZnO nanoparticles possess increased piezoelectric properties over ZnO micron particles. Due to this promise in neural applications, the objective of the present *in vitro* study was, for the first time, to assess the activity of astroglial cells on ZnO nanoparticle polymer composites. ZnO nanoparticles embedded in polyurethane were analyzed via scanning electron microscopy to evaluate nanoscale surface features of the composites. The surface chemistry was characterized via X-ray photoelectron spectroscopy. Astroglial cell response was evaluated based on cell adhesion and proliferation. Astrocyte adhesion was significantly reduced on ZnO nanoparticle/polyurethane (PU) composites with a weight ratio of 50:50 (PU:ZnO) wt.%, 75:25 (PU:ZnO) wt.%, and 90:10 (PU:ZnO) wt.% in comparison to pure PU. The successful production of ZnO nanoparticle composite scaffolds suitable for decreasing astroglial cell density demonstrates their potential as a nerve guidance channel material with greater efficiency than what may be available today.

Keywords: zinc oxide, nanoparticles, astrocytes, neural tissue, nervous system, biomaterials

Introduction

While peripheral nervous system (PNS) tissue is sometimes able to spontaneously regenerate after injury, damage to central nervous system (CNS) tissue cannot easily repair itself. To allow or enhance CNS repair, a nerve guidance channel (NGC) may be implanted around the damaged tissue. NGCs are essentially hollow tubes into which two severed ends of a nerve fiber bundle are inserted and sutured into place. The NGC provides an environment that promotes or accelerates tissue healing. Several materials have been considered for NGC fabrication including natural polymers such as collagen (Liu et al 1998) and synthetic polymers such as silicone and poly(lactic-co-glycolic) acid (PLGA) (Belkas et al 2004). NGCs may also be used in the PNS as well when injury is significant enough to result in a critical defect. Although autologous nerve grafts are the current gold standard treatment for PNS injury, the risk of infection and loss of neural tissue function at the donor site limit the success of this treatment option. Furthermore, synthetic grafts may be engineered to incorporate additional regeneration-stimulating cues, making them superior to autologous grafts.

Due to the complexity of tissue regeneration in the PNS and, particularly, the CNS, multifaceted solutions are necessary for the successful treatment of nerve injury.

Correspondence: Thomas J Webster
Division of Engineering,
Brown University, 182 Hope Street,
Providence, RI 02912 USA
Tel +1 401 863 2677
Fax +1 401 863 9107
Email thomas_webster@brown.edu

The inability of neural tissue to spontaneously regenerate, particularly in the CNS, is as much due to the presence of inhibitory cues as it is due to the absence of stimulatory cues. While a variety of strategies have delivered promising results, few attempts to treat injury in the PNS and CNS have implemented a combination of strategies. For example, bioactive molecular gradients, cell transplants, a variety of topographies, and electrical stimulation have all been individually investigated. For bioactive molecule strategies, nerve growth factor (NGF) and brain-derived neurotrophic factor (BDNF) have been shown to enhance axonal growth after spinal cord injury in rats (Bregman et al 1997). For cell-based strategies, Schwann cells, which promote tissue regeneration in the PNS, and olfactory ensheathing cells have been shown to enhance neural tissue regeneration when transplanted into the CNS (Schmidt et al 2003). Topographical guidance cues have also been shown to affect neural cell function, including micropatterned microgrooves in poly-D,L-lactic acid which promoted neurite alignment, particularly when coated with laminin (Miller et al 2002). Lastly, for electrical cues, direct current electrical stimulation is known to enhance and direct neurite outgrowth (McCaig et al 1991). Electrical fields as low as 10 mV/mm have been shown to guide neurite outgrowth (Rajnicek et al 1998). The direction of neurite outgrowth depended on cell type and the surface onto which the cells were cultured. An *in vivo* model using dogs with injured spinal cords showed that an oscillating electrical field of 500–600 mV/mm significantly accelerated the return of sensory and motor function after six weeks with futher recovery after six months (Borgens et al 1999). While the mechanisms by which electrical stimulation enhances neural cell activity are not entirely understood, studies have shown that electrical current passed through substrates (such as electrically conducting polypyrrole) can promote fibronectin protein adsorption that enhances neural cell activity *in vitro* (Kotwal et al 2001). Conductive (Schmidt et al 1997; Zhang et al 2007) and piezoelectric (Aebischer et al 1987) materials such as polyvinylidene fluoride have been shown to enhance neurite outgrowth and axonal regeneration without any external electrical stimulation.

Two of the above mentioned stimulatory cues, topographical and piezoelectric characteristics, are of particular interest. Although the incorporation of nanoscale (Webster et al 2004) and piezoelectric (Aebischer et al 1987) elements into NGC material candidates have both independently been shown to enhance neural regeneration, their combined effect is not yet known. In comparison to pure polymers, composites incorporating zinc oxide (ZnO) nanoparticles with a diameter near 60 nm could provide a scaffold for tissue regeneration that more closely resembles the scale of the building blocks that form natural neural support tissue. The size of laminin, collagen, and fibronectin, which are major components of the neural extracellular matrix (ECM), is on the same order of magnitude as a ZnO nanoparticle. Moreover, the piezoelectric characteristics of ZnO could allow for a transient electrical charge across the guidance channel upon mechanical deformation of the material. This could potentially be achieved via transcutaneous ultrasound stimulation of the guidance channel. Moreover, nanoscale ZnO has been shown to reduce the adhesion and density of staphylococcus epidermidis bacteria that is found naturally on the skin (Colon et al 2006). A significant reduction in the number of bacteria colony forming units has been shown on compacts of nanoscale ZnO compared to both compacts of microphase ZnO and to titania (Colon et al 2006). Although that study investigated ZnO primarily for its applications in orthopedic implant material design, the risk of bacterial infection exists for all implanted biomaterials. Antibacterial properties are equally desirable for implants designed to promote neural tissue regeneration. The combination of these characteristics into one nanostructured scaffold could produce the necessary electrical and topographical cues (along with a desirable antibacterial property) for axonal guidance and nervous system tissue regeneration.

Importantly, nanomaterials are intriguing for neural applications not only because they mimic the natural tissue roughness, but also due to their unique surface energetic and interactions with proteins. Specifically, enhanced adsorption of select proteins is believed to be the basis for enhanced cell functions on nanomaterials. Studies have shown greater neural cell (PC-12) adhesion, osteoblast adhesion, and ECM synthesis to nanomaterials compared to conventional materials with similar chemistry (Webster et al 2001, 2004; Khang et al 2007). Investigations of neural cell activity on carbon nanofibers revealed enhanced neurite outgrowth compared to cells cultured on conventional carbon fibers (McKenzie et al 2004). Biodegradable PLGA guidance channels consisting of submicron (>280 nm) fibers successfully permitted PNS tissue regeneration when implanted around a transected sciatic nerve (Panseri et al 2008). Increased cell adhesion has been attributed, in part, to greater amounts of fibronectin and vitronectin adsorbed to materials with greater surface roughness such as nanomaterials (Degasne et al 1999). Moreover,

further studies have shown that the proteins adsorbed to nanomaterial surfaces may expose more amino acid binding sequences than proteins adsorbed to conventional materials (Webster et al 2001). Specifically, vitronectin adsorbed to nanophase alumina demonstrated greater protein unfolding to expose amino acid binding sequences such as Arginine-Glycine-Aspartic Acid-Serine (RGDS) in comparison to vitronectin adsorbed to conventional alumina (Webster et al 2001). These studies have helped elucidate the mechanism for enhanced attachment of a variety of cell types to nanoscale biomaterials.

However, a number of cell types proliferate under non-physiological conditions or after injury. When a biomaterial is implanted in the body, immune responses may result in the proliferation of cells that serve to wall-off the material from the rest of the body. In the CNS, astroglial cells proliferate and produce an ECM protein-rich glial scar to isolate an implant (such as a neural electrode). Regeneration after injury in the CNS is inhibited primarily due to astrocytic glial scar formation. Outside of the CNS, an implanted biomaterial such as an orthopedic implant may attract fibroblast cells to the implant surface, compromising osseointegration. In these situations, nanomaterials have been shown to reduce the activity of undesirable cells. Studies evaluating astrocyte and fibroblast activity on carbon nanofibers have revealed reduced cell adhesion and proliferation compared to carbon fibers with diameters greater than the nanoscale (McKenzie et al 2004).

As a first attempt to examine ZnO nanoparticles and polymer composites as a novel NGC material, the purpose of the present study was to investigate astroglial response to polyurethane (PU) with embedded ZnO nanoparticles. Such a material provides the unique properties of ZnO in a polymer base that is flexible, biocompatible, and easy to fabricate. The surface energy, topographical, and chemical characteristics of ZnO/PU composites were investigated along with astroglial cell density on composite surfaces. This study was performed for the purpose of producing and investigating the next-generation of NGC materials that can minimize the inhibitory cues associated with astrocyte activity.

Materials and methods

Sample preparation

Composite materials composed of ZnO nanoparticles (~60 nm diameter, Nanophase Technologies, Romeoville, IL) and PU (Tecoflex medical grade SG80A, 90–140 $\times 10^3$ MW, Thermedics, Wilmington, MA) were produced with a range of weight ratios. Specifically, 50:50, 75:25, 90:10, 98:2, and 100:0 (PU:ZnO wt.%) were produced by mixing appropriate amounts of PU and ZnO nanoparticle stock solutions. The PU stock solution was prepared by dissolving 0.1 g PU in 13 ml chloroform (Sigma Aldrich, St. Louis, MO) during sonication (Sonicator 3000, Misonix, Farmingdale, NY). The ZnO nanoparticle stock solution was prepared by dispersing 0.1 g ZnO nanoparticles in 13 ml 1, 2-dichloroethane (Sigma Aldrich) during sonication. A range of solutions were mixed to provide the appropriate weight ratios and sonicated for 2 h at a power of 3 W to ensure nanoparticle dispersion. Solutions were then immediately pipetted onto 18 mm glass coverslips (Fisher Scientific, Pittsburgh, PA) and dried in a vacuum oven. To ensure evaporation of solvents, samples were left in an oven overnight at 50 °C in a vacuum of –10″ Hg. All samples were rinsed with ethanol and exposed to UV light prior to characterization or cell culture experiments.

Surface characterization

Sample surface morphology was viewed at a magnification of 6,000X and 30,000X using a scanning electron microscope (SEM; Hitachi 2700, Hitachi High-Technologies, Berkshire UK) at an accelerating voltage of 5 kV. Images were captured and analyzed with a Quartz PCI digital imaging system (Quartz Imaging Corporation, Vancouver, BC). Samples were fixed to aluminum specimen mounts (Electron Microscopy Sciences, Hatfield, PA) with double coated carbon tape and sputter coated prior to imaging. The sputter coater (Emitech K-550, Quorum Technologies, East Sussex, UK) provided a 15 nm AuPd layer by coating for 2 min at 20 mA when positioned at a height of 45 mm.

Surface chemistry of each sample was analyzed to determine the area of coverage of the respective elements at the sample surface. Following a brief sputter cleaning cycle, X-ray photoelectron spectroscopy (XPS; 5500 Multitechnique Surface Analyzer, Perkin Elmer, Waltham, MA) was used to detect the composition of the surface of each sample. XPS analysis parameters were adjusted to provide a sampling depth of approximately 50 Å over a circular area with a diameter of 1.1 mm. Information was acquired and analyzed with acquisition software (PC Access ESCA V7.2C, Physical Electronics, Chanhassen, MN). This information allowed for the estimation of the amount of nanoparticles exposed at the sample surface.

Surface energy calculation

Material surface energy and wettability were investigated with a drop shape analysis system (EasyDrop, Kruss, Hamburg, Germany). The contact angle of 10 µl sessile

droplets was measured at three locations on each of three samples. To determine surface energy, the contact angles of three different liquids (Deionized water, 1, 2-dichloroethane [Sigma Aldrich] and polyethylene glycol 2000 [PEG 2000; Sigma Aldrich]) were measured on each weight ratio sample. Measurements were taken 5s after placing the droplet on the sample surface. Drop shape analysis software (DSA2, Kruss, Hamburg, Germany) was used to calculate surface energy by entering surface tension and contact angle data into the Owens–Wendt equation.

Cell culture studies

Rat astrocytes (CRL-2005, American Type Culture Collection [ATCC], Manassas, VA) were cultured in Dulbecco's Modified Eagle Medium (DMEM; ATCC, Manassas, VA) supplemented with 10% fetal bovine serum (FBS; Hyclone, Logan, UT) and 1% penicillin/streptomycin (PS; Hyclone, Logan, UT) at 37 °C in a humidified environment of 5% CO_2/95% air. Cells were passaged 4–5 times before seeding the substrates.

Astrocyte adhesion

Astrocytes were detached from the culture flasks with trypsin and collected in a conical tube for centrifugation. Cell pellets were resuspended in 1 ml DMEM and counted using a hemocytometer. The number of cells needed to seed samples at a density of 5000 cells/cm^2 was resuspended in a volume of 400 µl of cell media per sample. Cell-seeded samples in a 12-well plate were carefully transferred to an incubator and left for 4 h. After 4 h, the media was aspirated from the wells and the samples were rinsed with phosphate-buffered saline (PBS) to remove all nonadherent cells. Calcein-AM (BD Biosciences, San Jose, CA) was added to each sample at a concentration of 0.5 µM in PBS. After 30 min, samples were rinsed again with PBS before imaging on a fluorescence microscope. Five images were taken at random locations on each sample. Images were analyzed with Image J software (NIH, Bethesda, MA) to determine cell density.

Astrocyte proliferation

Astrocytes were collected and counted following the same procedures described for the adhesion assays. Specifically, 2500 cell/cm^2 were resuspended in 400 µl of cell media per sample and placed on each substrate. Seeded substrates in a 12-well plate were carefully transferred to an incubator and left for 24, 48, or 72 h. Media was changed daily for samples incubated for 48 and 72 h. After incubation, cells were stained with Calcein-AM (BD Biosciences) following the same protocol as reported for the adhesion assays.

Statistical analyses

Numerical data were analyzed for significance using the student's *t*-test. Values are reported as the mean ± SEM. The threshold for significance was set at $p < 0.05$.

Results

SEM and XPS analyses

Sample characterization via SEM (Figure 1) and XPS (Table 1) suggested that the ZnO nanoparticles exposed on the composite surface contributed to larger amounts of nanoroughness. While SEM images revealed nanoscale features of individual ZnO nanoparticles at or near the material surface, XPS analysis confirmed that the particles were in fact at the

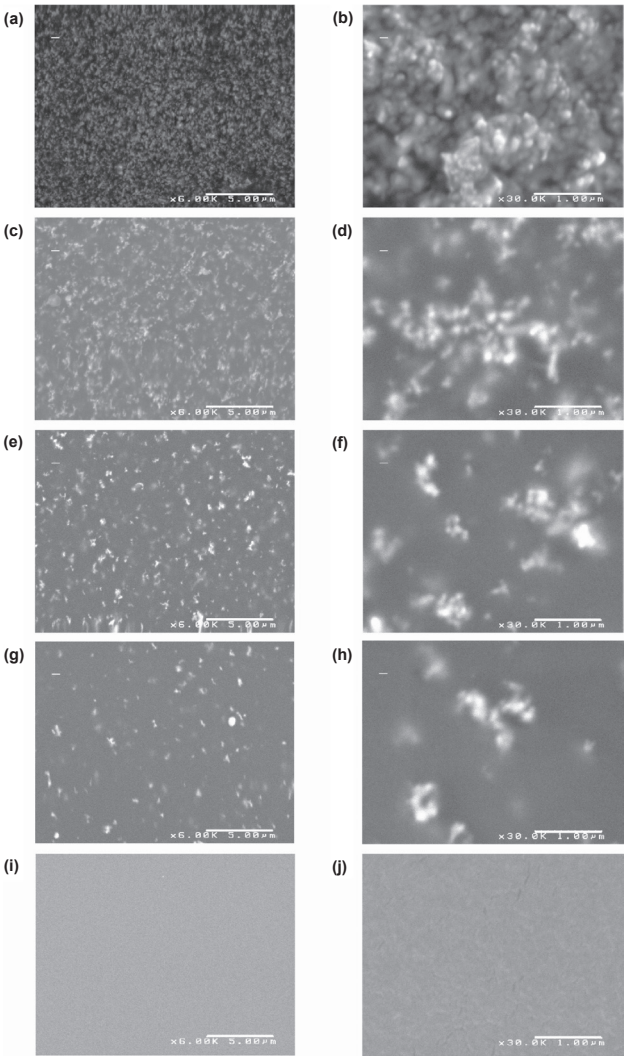

Figure 1 Scanning electron micrographs of the ZnO/PU composites. 50:50 (PU:ZnO) wt.% at 6,000X (**a**) and 30,000X (**b**); 75:25 (PU:ZnO) wt.% at 6,000X (**c**) and 30,000X (**d**); 90:10 (PU:ZnO) wt.% at 6,000X (**e**) and 30,000X (**f**); 98:2 (PU:ZnO) wt.% at 6,000X (**g**) and 30,000X (**h**); 100:0 (PU:ZnO) wt.% at 6,000X (**i**) and 30,000X (**j**).
Notes: Scale bar for images in left column = 5 µm. Scale bar for images in right column = 1 µm.

Table 1 X-ray photoelectron spectroscopy data for ZnO/PU composites. Zinc was detected at the surface for samples with weight ratios of 50:50 (PU:ZnO) wt.% and 75:25 (PU:ZnO) wt.%. No zinc was detected at the surface of samples with a lower concentration of ZnO nanoparticles

Weight ratio (PU:ZnO)	ZnO surface area (% coverage)
100:0	ND
98:2	ND
90:10	ND
75:25	2.11
50:50	3.98

Abbreviation: ND, not detectable.

material surface and were not coated by the polymer. SEM images suggested that as ZnO nanoparticle concentration increased, surface nanofeatures of the sample also increased. At lower concentrations, nanoparticle agglomeration was more evident in SEM images. XPS analysis indicated that as the nanoparticle concentration increased, more zinc was exposed at the material surface. Zinc was detected at the surface of the composites at weight ratios of 50:50 (PU:ZnO) wt.% and 75:25 (PU:ZnO) wt.%. Zinc was not detected at the surface of the composites at weight ratios of 90:10 (PU:ZnO) wt.% or 98:2 (PU:ZnO) wt.%. However, since XPS is unable to confirm the presence of an element at very lower concentrations, this did not confirm the absence of zinc at the surface of these samples. By extrapolating from XPS data which indicated that zinc covered 3.98% of the surface of a sample with a weight ratio of 50:50 (PU:ZnO) wt.% and 2.11% of the surface of a sample with a weight ratio of 75:25 (PU:ZnO) wt.%, it was estimated that the area of zinc coverage for the 90:10 (PU:ZnO) wt.% and 98:2 (PU:ZnO) wt.% composites could be less than 1% of the surface area. With a coverage area this low, the XPS system may not have been able to accurately detect the presence of zinc.

Sample surface energy

Surface energy calculations from contact angle data indicated that adding ZnO nanoparticles to PU increased sample surface energy. Samples with weight ratios of 50:50 (PU:ZnO) wt.%, 75:25 (PU:ZnO) wt.%, 90:10 (PU:ZnO) wt.% and 98:2 (PU:ZnO) wt.% had a surface energy significantly higher than the pure polymer (Figure 2). These samples had a lower contact angle for each liquid as the ZnO nanoparticle concentration increased (Table 2). Incorporation of ZnO nanoparticles significantly increased surface energy and wettability of PU at all nanoparticle concentrations. For samples with weight ratios of 50:50 (PU:ZnO) wt.% and 75:25 (PU:ZnO) wt.%, surface energy was significantly higher in comparison to samples with a weight ratio of 90:10 (PU:ZnO) wt.%.

Astrocyte adhesion and proliferation

Lastly, results of this study showed a reduced ability of astrocytes to adhere and proliferate on ZnO nanoparticle PU

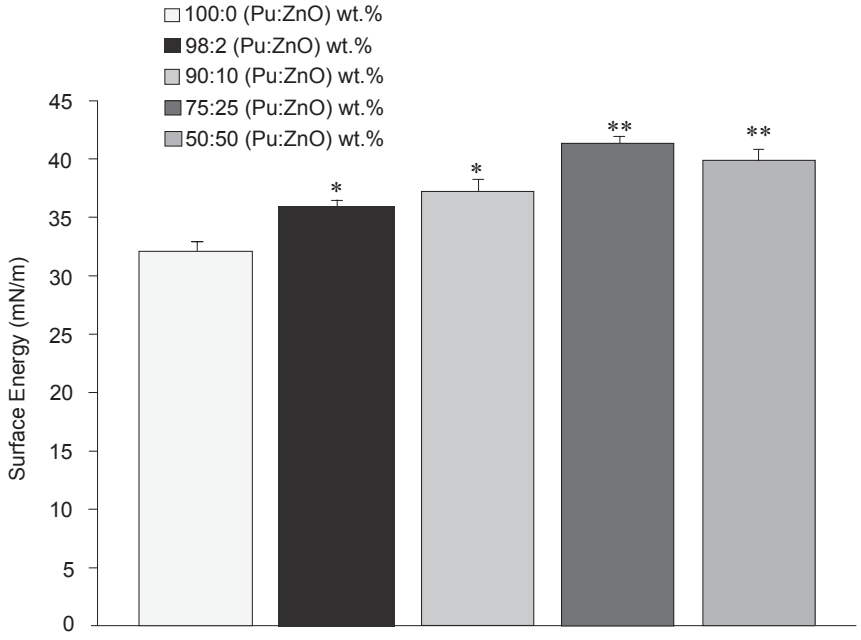

Figure 2 Surface energy of ZnO/PU composites. Surface energy was calculated for each sample by measuring the contact angle of three liquids at the sample surface and entering values into the Owens-Wendt equation.
Notes: Values are mean ± SEM; n = 3; *$p < 0.05$ (compared to 100:0 [PU:ZnO] wt.%), **$p < 0.05$ (compared to 90:10 [PU:ZnO] wt.%).

Table 2 Contact angles of three liquids on sample surfaces. Contact angle data was used to determine surface energy via the Owens-Wendt equation

Weight ratio (PU:ZnO)	Contact angle of DI water	Contact angle of 1,2-dichloroethane	Contact angle of PEG 2000
100:0	86.51 ± 0.19	31.56 ± 2.42	55.88 ± 3.48
98:2	81.75 ± 2.24	26.34 ± 1.42	51.14 ± 1.96
90:10	80.08 ± 0.47	24.08 ± 1.37	47.6 ± 1.93
75:25	77.71 ± 1.51	21.33 ± 3.06	43.38 ± 2.07
50:50	73.49 ± 1.73	16.41 ± 0.029	36.51 ± 0.82

Note: Values are mean ± SEM.

composites with higher nanoparticle concentrations. Cell images captured after a 4 h adhesion assay illustrated reduced astrocyte cell density as ZnO nanoparticle concentration increased (Figure 3). At 4 h, cell adhesion was significantly reduced on samples with weight ratios of 50:50 (PU:ZnO) wt.%, 75:25 (PU:ZnO) wt.%, and 90:10 (PU:ZnO) wt.% compared to the pure polymer (Figure 4). Increased concentrations of nanoparticles in ZnO/PU composites also reduced cell proliferation. At 24, 48, and 72 h, cell density was reduced on samples with weight ratios of 50:50 (PU:ZnO) wt.%, 75:25 (PU:ZnO) wt.%, and 90:10 (PU:ZnO) wt.% compared to pure polymers at the same time point (Figure 5). At all time points, cell density of samples with weight ratios of 50:50 (PU:ZnO) wt.% and 75:25 (PU:ZnO) wt.% was further reduced compared to composites with weight ratios of 90:10 (PU:ZnO) wt.%. At 72 h, cell density on samples with weight ratios of 50:50 (PU:ZnO) wt.% was reduced compared to cell density on samples of the same composition at the 24 h time point.

Discussion

There are a number of fundamental reasons why nanomaterials are well suited for tissue engineering applications. First, nanomaterials are biomimetic. In other words, materials

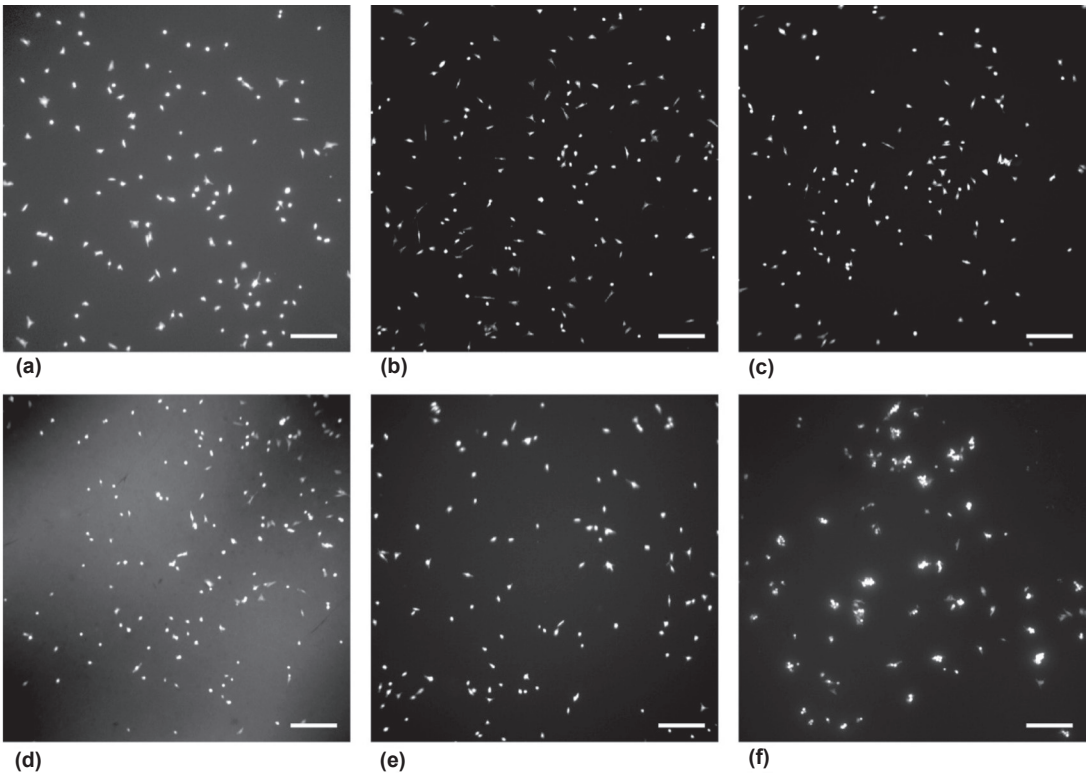

Figure 3 Fluorescence microscope images of astrocyte adhesion after 4 h. Astrocytes were seeded at a density of 5000 cells/cm^2 on each sample for 4 h. Cells seeded on glass (**a**), 100:0 (PU:ZnO) wt.% (**b**), 98:2 (PU:ZnO) wt.% (**c**), 90:10 (PU:ZnO) wt.% (**d**), 75:25 (PU:ZnO) wt.% (**e**), and 50:50 (PU:ZnO) wt.% (**f**).
Notes: Samples were stained with Calcein-AM prior to imaging. Scale bar = 200 μm.

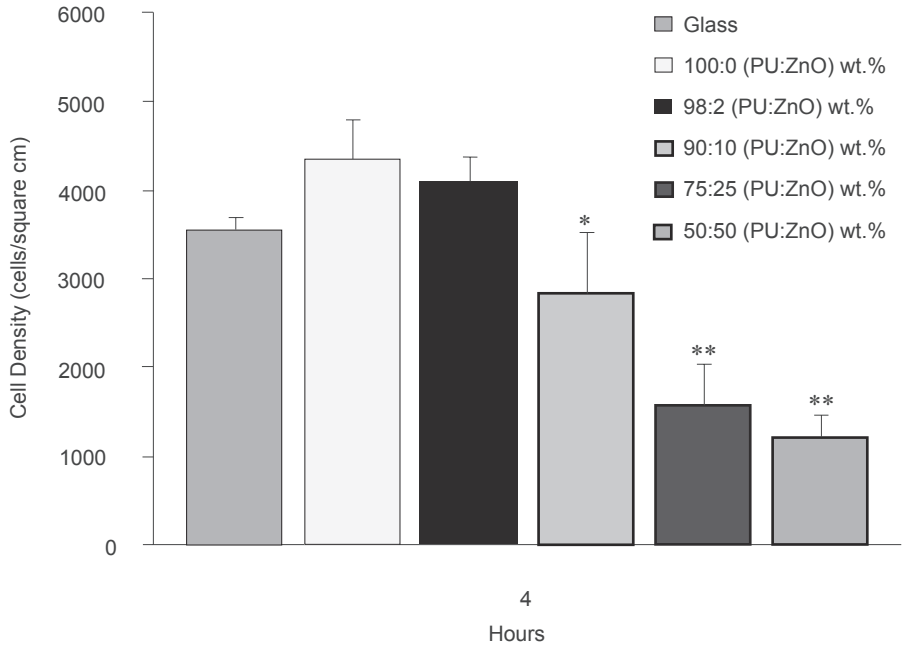

Figure 4 Results of astrocyte 4 h adhesion assay. 5000 cells/cm^2 were seeded on each sample and incubated for 4 h. Cell density was determined from images taken at five random locations on each sample.
Notes: Values are mean ± SEM; n = 3; *p < 0.05 (compared to 100:0 [PU:ZnO] wt.%), **p < 0.05 (compared to 90:10 [PU:ZnO] wt.%).

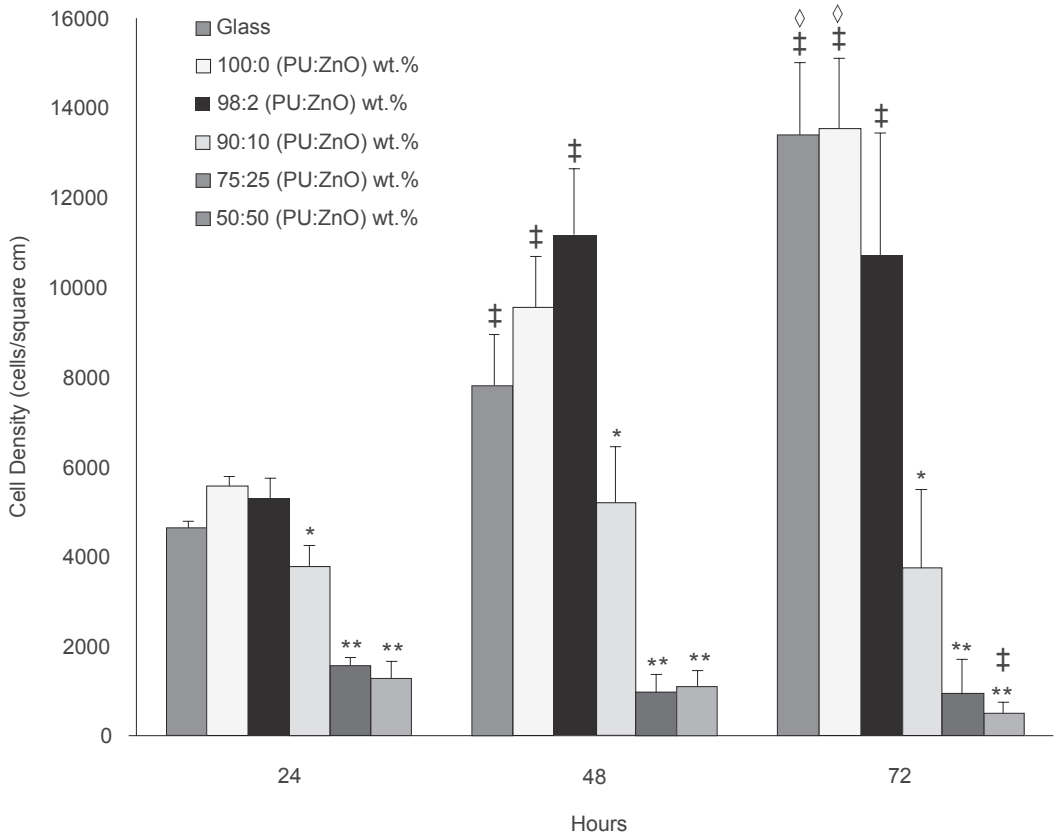

Figure 5 Results of 1, 2, and 3 day astrocyte proliferation assay. Cells were seeded at t = 0 with 2500 cells/cm^2. Values are mean ± SEM; n = 3; *p < 0.05 (compared to 100:0 [PU:ZnO] wt.% at the same time point), **p < 0.05 (compared to 90:10 [PU:ZnO] wt.% at the same time point), ‡p < 0.05 (compared to same sample composition at the 24 h time point), ◊p < 0.05 (compared to same sample composition at 48 h time point).

with nanoscale surface features more accurately mimic the nanoscale proteins which compose biological tissue. Second, engineering a material to exhibit nano-roughness provides a greater functional surface area for interaction with surrounding cells and tissue. This increased surface area allows for increased select protein adsorption, a critical intermediate step in the adhesion and function of cells (Webster et al 2001). Third, due to an increase in grain boundaries, nanomaterials have greater surface energy than their conventional counterparts. Not only can this promote greater protein adsorption, it also may provide the proper environment for the ideal protein conformation, and thus bioactivity (Khang et al 2007).

Data from this study indicated that surface energy increased with increased concentrations of ZnO nanoparticles in the polymer composite. Samples with a range of surface energies would be expected to interact differently with proteins. Changes in protein adsorption and conformation due to increased surface energy may begin to explain alterations in astrocyte cell density on samples with high concentrations of ZnO nanoparticles. Although cell interactions with implanted biomaterials show us that cells do not adhere directly to the material, but rather to proteins that have adsorbed to its surface, biomimetic materials provide a better physiological foundation for protein interactions. Nanomaterials allow for adsorbed proteins to more accurately recreate the ECM. The importance of altered protein interactions (including both adsorption and conformation) with nanostructured compared to conventional material surfaces helps to explain why cells behave differently on these respective materials. That is, adsorption of proteins to other proteins or to a surface which has similar roughness to proteins (ie, a nanostructured surface) may be superior to cells which adhere to proteins adsorbed to a nonbiologically inspired nanosmooth surface.

To appreciate why biomimetic materials provide superior tissue engineering surfaces, the role that the ECM plays in regulating cell function must be understood. All cells exist within an ECM, the proteins that provide structural support for a biological tissue. ECM proteins interact with cell surface receptors to regulate gene expression and cell function. Conventional biomaterials with surface features on a micron scale do not resemble the ECM and, thus, are not biomimetic. Cellular interactions with nanoscale biomaterials may provide a more physiological activation of cell surface receptors for a more physiological cellular function.

Non-physiological conditions in the CNS may be identified and initiate an aggressive immune response. For example, upon implantation of a neural electrode composed of conventional materials, it is recognized as foreign. Activated astrocytes begin proliferating producing a thick ECM to create a glial scar surrounding the implant. Neural electrodes composed of nanomaterials have been shown to reduce glial scar and reduce impedance around the electrode for longer periods of time (Moxon et al 2004). This phenomenon is equally beneficial in regards to NGC implantation. Successful neural tissue regeneration requires the minimization of the glial scar, a physical and chemical barrier that prevents neural tissue regeneration in the CNS. This study indicated that astrocyte activity was minimized on composites composed of ZnO nanoparticles and PU, an important factor in the ability of this material to serve as a NGC component. Although stimulatory cues that promote neural cell growth and function are critical aspects of neural tissue regeneration, this study has demonstrated that the inhibitory cues that prevent spontaneous recovery after neural tissue injury, such as astrocyte activity, can possibly be reduced on nanomaterials. The piezoelectric properties of the ZnO nanoparticles in these composites, which have yet to be investigated, may be enhanced due to the large surface to volume ratio inherent to nanoparticles (Xiang et al 2006). Atoms in the nanoscale ZnO structures are able to assume different positions, due to the free boundary, which may enhance the piezoelectric effect. A significant piezoelectric response from these composites may provide the stimulatory cues necessary to promote neural cell function.

Conclusions

ZnO nanoparticle and polymer composites incorporate elements from a number of current strategies for neural tissue repair (such as nanotopography and piezoelectric properties) to create a new approach to promote nervous tissue regeneration. The next generation of NGCs can benefit from the incorporation of nanomaterials that provide a superior environment for protein adsorption and cell activity. Sample characterization revealed that ZnO/PU composites can be fabricated to create substrates with increased surface energy and nanoroughness at the sample surface. Importantly, this study showed for the first time that these samples reduced the adhesion and proliferation of astroglial cells. The piezoelectric activity of these samples must be investigated to evaluate the electrical stimulus that could be created by mechanically deforming the scaffold. These particular nanorough piezoelectric samples may combine a number of known regeneration-stimulating cues, making them superior to non-piezoelectric nanomaterials, conductive materials, or conventional piezoelectric materials alone. Future studies

with these samples will evaluate protein adsorption, neural cell activity, and the piezoelectric response to mechanical deformation of the composites.

Acknowledgments

The authors would like to thank the National Science Foundation for fellowship support (Brown University GK-12) and the Hermann Foundation for funding. The authors thank Mike Platek of the University of Rhode Island for XPS assistance and Geoffrey Williams of the Leduc Bioimaging Facility at Brown University for SEM assistance.

References

Aebischer P, Valentini RF, Dario P, et al. 1987. Piezoelectric guidance channels enhance regeneration in the mouse sciatic nerve after axotomy. *Brain Res*, 436:165–8.

Belkas JS, Shoichet MS, Midha R. 2004. Peripheral nerve regeneration through guidance tubes. *Neurol Res*, 26:151–60.

Borgens RB, Toombs JP, Breur G, et al. 1999. An imposed oscillating electrical field improves the recovery of function in neurologically complete paraplegic dogs. *J Neurotrauma*, 16:639–57.

Bregman BS, McAtee M, Dai HN, et al. 1997. Neurotrophic factors increase axonal growth after spinal cord injury and transplantation in the adult rat. *Exper Neurol*, 148:475–94.

Colon G, Ward BC, Webster TJ. 2006. Increased osteoblast and decreased staphylococcus epidermidis functions on nanophase ZnO and TiO2. *J Biomed Mater Res A*, 78:595–604.

Degasne I, Basle MF, Demais V, et al. 1999. Effects of roughness, fibronectin and vitronectin on attachment, spreading, and proliferation of human osteoblast-like cells (saos-2) on titanium surfaces. *Calcif Tissue Int*, 64:499–507.

Khang D, Sung Yeol K, Liu-Snyder P, et al. 2007. Enhanced fibronectin adsorption on carbon nanotube/poly(carbonate) urethane: Independent role of surface nano-roughness and associated surface energy. *Biomaterials*, 28:4756–68.

Kotwal A, Schmidt CE. 2001. Electrical stimulation alters protein adsorption and nerve cell interactions with electrically conducting biomaterials. *Biomaterials*, 22:1055–64.

Liu S, Bodjarian N, Langlois O, et al. 1998. Axonal regrowth through a collagen guidance channel bridging spinal cord to the avulsed C6 roots: Functional recovery in primates with brachial plexus injury. *J Neurosci Res*, 51:723–34.

McCaig CD, Rajnicek AM. 1991. Electrical fields, nerve growth, and nerve regeneration. *Exper Physiol*, 76:473–94.

McKenzie JL, Waid MC, Shi R, et al. 2004. Decreased functions of astrocytes on carbon nanofiber materials. *Biomaterials*, 25:1309–17.

Miller C, Jeftinija S, Mallapragada S. 2002. Synergistic effects of physical and chemical guidance cues on neurite alignment and outgrowth on biodegradable polymer substrates. *Tissue Eng*, 8:367–78.

Moxon KA, Kalkhoran NM, Markert M, et al. 2004. Nanostructured surface modification of ceramic-based microelectrodes to enhance biocompatibility for a direct brain-machine interface. *IEEE Trans Biomed Eng*, 51:881–9.

Panseri S, Cunha C, Lowery J, et al. 2008. Electrospun micro-and nanofiber tubes for functional nervous regeneration in sciatic nerve transections. *BMC Biotech*, 8:39–51.

Rajnicek AM, Robinson KR, McCaig CD. 1998. The direction of neurite growth in a weak DC electric field depends on the substratum: contributions of adhesivity and net surface charge. *Dev Biol*, 203:412–23.

Schmidt CE, Leach JB. 2003. Neural tissue engineering: Strategies for repair and regeneration. *Ann Rev Biomed Eng*, 5:293–347.

Schmidt CE, Shastri VR, Vacanti JP, et al. 1997. Stimulation of neurite outgrowth using an electrically conducting polymer. *Proc Natl Acad Sci U S A*, 94:8948–53.

Webster TJ, Waid MC, McKenzie JL, et al. 2004. Nano-biotechnology: Carbon nanofibres as improved neural and orthopaedic implants. *Nanotechnology*, 15:48–54.

Webster TJ, Schadler LS, Siegel RW, et al. 2001. Mechanisms of enhanced osteoblast adhesion on nanophase alumina involve vitronectin. *Tissue Eng*, 7:291–301.

Webster TJ, Ejiofor JU. 2004. Increased osteoblast adhesion on nanophase metals: Ti, Ti6Al4V, and CoCrMo. *Biomaterials*, 25:4731–39.

Xiang HJ, Yang J, Hou JG, et al. 2006. Piezoelectricity in ZnO nanowires: A first-principles study. *Appl Phys Lett*, 89:223111–3.

Zhang Z, Rouabhia M, Wang Z, et al. 2007. Electrically conductive biodegradable polymer composite for nerve regeneration: Electricity-stimulated neurite outgrowth and axon regeneration. *Artif Organs*, 31:13–22.